Chemistry & Biology, Vol. 11, 1659–1666, December, 2004, ©2004 Elsevier Ltd. All rights reserved. DOI 10.1016/j.chembiol.2004.09.013

Membrane-Permeable and -Impermeable Sensors of the Zinpyr Family and Their Application to Imaging of Hippocampal Zinc In Vivo

Carolyn C. Woodroofe,[1] Rafik Masalha,[2] Katie R. Barnes,[1] Christopher J. Frederickson,[2] and Stephen J. Lippard[1,*]
[1]Department of Chemistry
Massachusetts Institute of Technology
Cambridge, Massachusetts 02139
[2]NeuroBioTex, Inc.
101 Christopher Columbus Boulevard
Galveston, Texas 77550

Summary

Esterification of fluorescent biosensors is a common strategy used to trap probes within the cell. Zinpyr-1 (ZP1) is a fluorescein-based bright fluorescent sensor for divalent zinc that is cell permeable without prior modification. We describe here the synthesis and characterization of ZP1 sensors containing a carboxylic acid or ethyl ester functionality at the 5 or 6 position of the fluorescein. The presence of an electronegative carboxylate decreases the proton-induced background fluorescence of the probe by lowering the pK_a of the benzylic amines responsible for fluorescence quenching. The charged species ZP1(6-CO_2^-) is membrane-impermeant, whereas the permeability of the neutral ZP1(5/6-CO_2Et) is similar to that of the parent sensor. Intracranial microinfusion of ZP1(6-CO_2Et) into rat hippocampus produces reduced staining of vesicular zinc in neuropil and very clear delineation of zinc-positive injured neuronal somata and dendrites as compared with ZP1.

Introduction

The synthesis of fluorescent sensors for biological imaging of Zn^{2+} has drawn a great deal of recent attention [1–3]. Intracellular Zn^{2+} is a key structural or catalytic component of many proteins, with the overall intracellular concentration estimated to average 150 μM [4]. A complex system of zinc transporter proteins is employed in order to control Zn^{2+} homeostasis [5, 6], and the vast majority of intracellular Zn^{2+} is sequestered or tightly bound to proteins such that cytosolic chelatable Zn^{2+} is essentially nonexistent [7]. Certain specialized areas of the body accumulate Zn^{2+}. The presence of low millimolar concentrations of loosely bound Zn^{2+} in CA3 synaptic vesicles of the mammalian cerebral cortex is of particular interest. This vesicular Zn^{2+}, which constitutes about 8% of total brain zinc, is conspicuous in hippocampal mossy fiber boutons and has been demonstrated by autometallographic and fluorescence techniques [8]. Extensive experimentation has not established definitively the normal physiological roles of hippocampal synaptic zinc [9, 10]; however, a modulatory role in seizure conditions [11] and subsequent neuronal damage is indicated [12, 13]. Because Zn^{2+} is a spectroscopically silent metal ion, fluorescent sensing approaches to studying the movements and functions of brain zinc ion are of great utility.

There are three areas in which rapidly exchangeable, loosely bound zinc may be imaged in the brain: the cytosol, secretory storage granules including neuronal vesicles, and in the extracellular fluids. Membrane-impermeant dyes are useful for imaging extracellular Zn^{2+} released from presynaptic terminals [14], whereas sequestered vesicular Zn^{2+} is best imaged with a stably lipophilic probe. Detection of cytosolic free Zn^{2+}, which appears almost exclusively in injured or oxidatively stressed neurons, is best achieved with a trappable probe.

Among the list of desirable properties [15] for a fluorescent biosensor is the ability to permeate into the cell and subsequently become trapped. This "trappable" property is most often achieved by the inclusion of an ester moiety [16]. The lipophilic ester enters the cell and is hydrolyzed by intracellular esterases to a charged, membrane-impermeant carboxylate. Ethyl esters and the more hydrolytically labile acetoxymethyl esters [17] are most commonly used for this purpose. One relevant example of this strategy is its application to the *p*-toluenesulfonamidoquinoline (TSQ) family of Zn^{2+} sensors. TSQ is lipophilic and penetrates both plasma and vesicular membranes, readily staining vesicular zinc in tissue [18]; however, this probe is primarily applied as a histochemical stain rather than a probe for living tissue because of the harsh conditions of the standard staining protocol [19]. The TSQ-based sensor Zinquin, which contains an ethyl ester to aid in solubilizing and retaining the sensor in cells, was designed and synthesized [20]; subsequent results suggest that the free acid form is also membrane permeable [21]. The presence of the ester group does not noticeably affect intracellular staining of mouse LTK fibroblasts compared to an analogous sensor containing a 6-methoxy group (2-Me-TSQ) [22].

The fluorescein-based Zn^{2+} sensor Zinpyr-1 (ZP1, Figure 1) has recently been reported [23]. This sensor is excited by low-energy visible light (λ_{max} > 500 nm), is extremely bright (ϕ_{Zn} = 0.87, ϵ_{Zn} = 8.4 × 10^4 $M^{-1}cm^{-1}$), and is membrane permeable without prior modification. A second generation of Zinpyr sensor, which does not enter intact cells, has been introduced and is exemplified by the asymmetric molecule ZP4 (Figure 1). Their permeability has been exploited in the selective imaging of damaged neurons [24, 25]. By changing the substituent X (X = F, Cl, OMe) in the ZP4 family, it has been possible to modulate their properties without altering the membrane permeability of these sensors [26]. In the present article we describe chemical routes to a trappable ZP1 with a hydrolyzable ethyl ester in order to examine the effects of this modification on subcellular localization in vitro and in vivo. Our chemistry furnishes both membrane-permeable and -impermeable, visible-excitation sensors, the preparation of which can be readily scaled up to afford multigram

*Correspondence: lippard@mit.edu

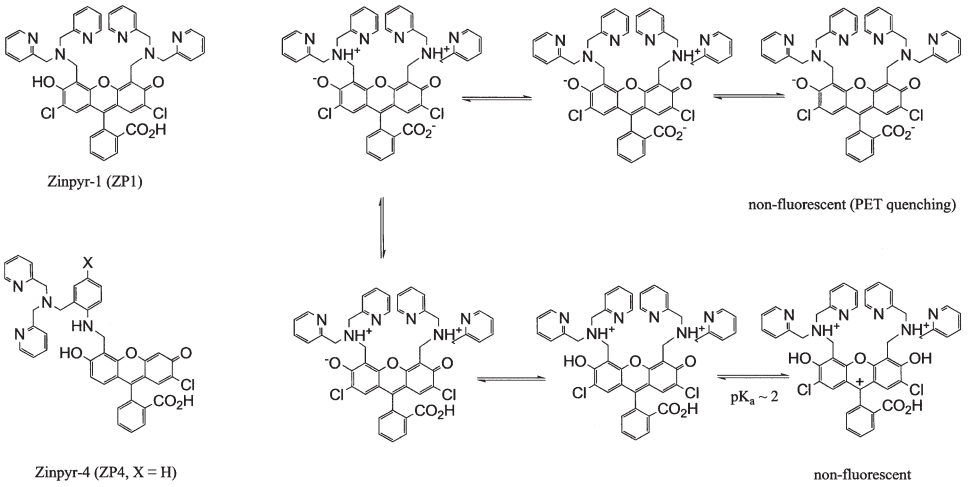

Figure 1. Structural Diagrams of ZP1 and ZP4 and Protonation Equilibria for the Former

quantities of material. Applications to imaging hippocampal zinc ion are also reported.

Results and Discussion

The basic structure of Zinpyr-1, depicted in Figure 1, contains chlorine atoms at the 2′ and 7′ positions of the fluorescein platform. In its metal-free form, the lone pair of a benzylic amine largely quenches the fluorescence of ZP1. Coordination of this amine to Zn^{2+} or protonation affords an approximately 3-fold increase in fluorescence. The dipicolylamine Zn^{2+} binding groups are installed via a Mannich reaction on the parent dichlorofluorescein. Substituents at the 2′ and 7′ positions are necessary to prevent Mannich reaction chemistry from occurring at these positions. A Mannich reaction of 5- or 6-carboxylate derivatives of 2′,7′-dichlorofluorescein was therefore carried out as a desirable route to ester- and acid-functionalized ZP1 derivatives. The dichlorofluorescein-5(6)-carboxylates were synthesized as a mixture of isomers (**1a, 1b**) by methanesulfonic acid-catalyzed fluorescein condensation of 4-chlororesorcinol with benzene tricarboxylic acid [27]. This reaction affords two isomers, owing to lack of selectivity between the acid moieties at the 1 and 2 positions of the starting benzenetricarboxylic acid. The product mixture was protected and separated as the diacetates **2a** and **2b**. Activation of **2a** and **2b** with oxalyl chloride and subsequent reaction with ethanol gave the fluorescein ethyl ester diacetates (**3a, 3b**) in 65%–70% yield, as shown in Figure 2. Esterification of either carboxylate with ethanol under Mitsunobu conditions was also effective. The desired ZP1 carboxylates (**4a,** ZP1(6-CO_2H) and **4b,** ZP1(5-CO_2H)) or esters (**5a,** ZP1(6-CO_2Et) and **5b,** ZP1(5-CO_2Et)) were isolated following Mannich reactions of the corresponding fluorescein diacetates **2a-b** or **3a-b** with dipicolylamine and paraformaldehyde (Figure 2). The isolated yields of ethyl esters **5a** and **5b** were reproducibly much lower (40%, 44%) than those of the free carboxylates **4a** and **4b** (73%,

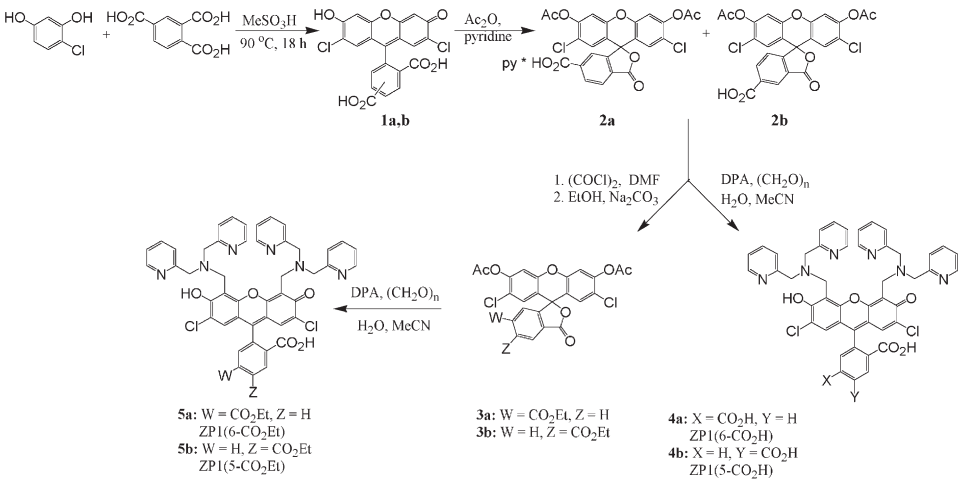

Figure 2. Synthesis of ZP1(5/6-CO_2R)

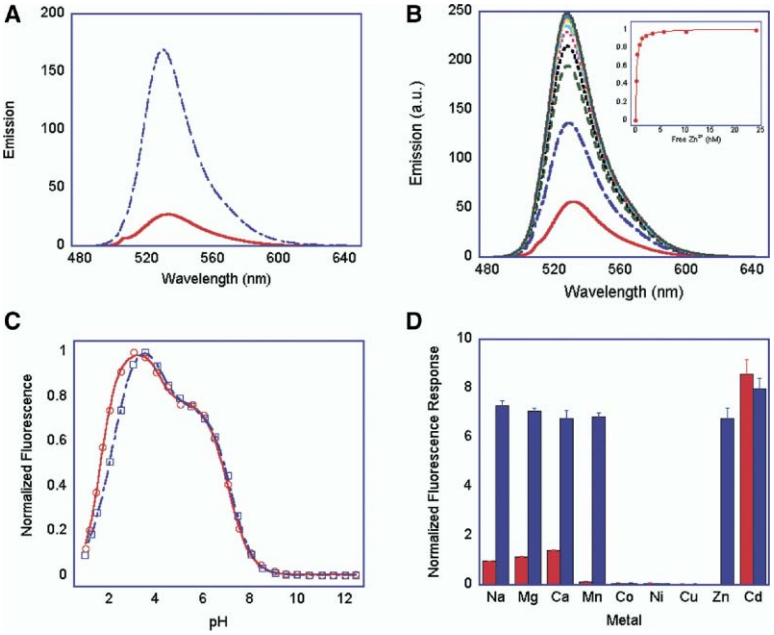

Figure 3. Chemical and Fluorescence Properties of ZP1(5/6CO_2H)

(A) Zn^{2+} response of ZP1(6-CO_2H) with excitation at 505 nm (pH 7.4).

(B) ZP1(6-CO_2H) response to nanomolar levels of free Zn^{2+}. Inset shows K_d fit.

(C) Fluorescence pH profile of ZP1(5-CO_2H) (circles) and ZP1(6-CO_2H) (squares).

(D) Selectivity of Zn^{2+} response: treatment of 1 μM dye with 50 μM–2 mM of shown metal ion (red bars) followed by addition of 50 μM $ZnCl_2$ (blue bars).

79%). We previously communicated the analogous synthesis and properties of a ZP1-derivatized sensor containing an amido functional group at the 6 position [28].

The physical properties of the new sensors and their zinc complexes were examined. Addition of Zn^{2+} to a 1 μM aqueous solution of each sensor afforded an increase in integrated emission up to 8-fold. The dissociation constant for the first binding event was determined by using a dual-metal EDTA buffered system, as previously described [29]. Representative data for K_{d1} measurements are provided in Figure 3. The presence of an electron-withdrawing carboxyl substituent at the 5 or 6 position has little effect on the binding affinity for Zn^{2+} relative to ZP1 (Table 1). Previous results have indicated that the first binding event is responsible for the large fluorescence increase and that the dissociation constant for binding a second zinc(II) ion to ZP1 is several orders of magnitude higher than the first [23]. The second dissociation constants were not measured in the present study.

Quantum yields of the sensors in the bound and free states were determined relative to a fluorescein standard. All four sensors have lower background fluorescence (ϕ = 0.13–0.21) in the free state compared with the parent ZP1 (ϕ = 0.38). This property may be related to diminished protonation of the benzylic amines, as discussed below. The brightness of the metal-bound sensors ZP1(5/6-CO_2R) is comparable to that of ZP1 (Table 1). Each sensor undergoes a blueshift in absorbance of ~10 nm upon Zn^{2+} binding. Extinction coefficients of the Zn^{2+} complex are increased over those of the free fluorophores in all cases by 10%–15%. The extinction coefficient for the Zn^{2+} complex of ZP1-6-CO_2H was determined at lower concentration, because the Beer's law plot is nonlinear above ~5 μM. This result may be due partly or wholly to formation of dye aggregates [30]. The brightness values of the free sensors are significantly reduced in comparison with the parent Zinpyr-1 sensor, whereas the brightness values of the Zn^{2+}-bound sensors are comparable, representing a decrease in background fluorescence and an increase in sensor dynamic range. Measured values are listed in Table 1.

Equilibrium constants for three protonation events that affect fluorescence were determined by titration fluorimetry. The pK_a at 7 corresponds to protonation of the benzylic amine responsible for PET quenching of the fluorescence. This value does not vary considerably

Table 1. Photochemical Constants of ZP1(5/6-CO_2R) in the Presence and Absence of Zn^{2+}

Sensor	λ_{max}(Abs, nm)	ϵ_{max}(M^{-1} cm^{-})	ϕ	Brightness[a]	K_{d1} Zn^{2+}(nM)	pK_{a1}	pK_{a2}	pK_{a3}
ZP1(5-CO_2Et)	517	66,000	0.14	9.2×10^3	0.26 ± 0.03	1.53(2)	4.02(3)	6.98(7)
+ Zn^{2+}	506	71,000	0.58	4.1×10^4				
ZP1(5-CO_2H)	520	81,000	0.17	1.4×10^4	0.22 ± 0.04	1.57(4)	3.7(4)	7.05(8)
+ Zn^{2+}	509	88,000	0.62	5.5×10^4				
ZP1(6-CO_2Et)	519	61,000	0.13	7.9×10^3	0.37 ± 0.04	2.1(1)	4.0(1)	7.00(4)
+ Zn^{2+}	509	72,000	0.67	4.8×10^4				
ZP1(6-CO_2H)	516	76,000	0.21	1.6×10^4	0.16 ± 0.02	2.12(1)	4.07(4)	7.12(7)
+ Zn^{2+}	506	81,000	0.63	5.1×10^4				
ZP1 [31]	515	79,500	0.38	3.0×10^4	0.7 ± 0.1	2.75		8.37
+ Zn^{2+}	507	84,000	0.87	7.3×10^4				

[a] Brightness is defined as the product of quantum yield and extinction coefficient at the maximum absorption ($\phi \times \epsilon_{max}$).

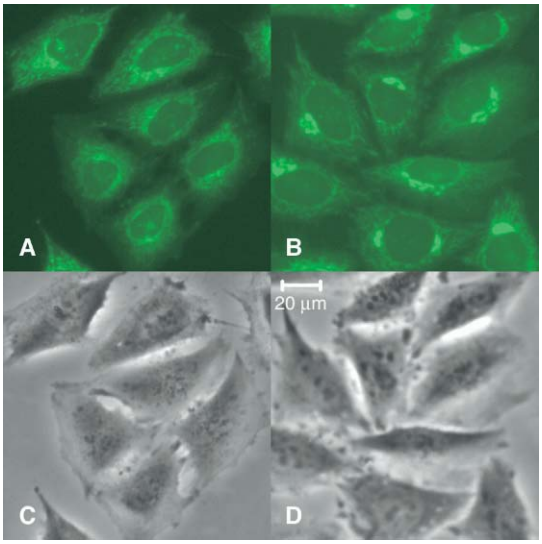

Figure 4. Comparison of ZP1-CO_2Et and ZP1 Staining

HeLa cells were incubated for 30 min at 37°C with 5 μM ZP1(6-CO_2Et) (A and C) or 5 μM ZP1 (B and D), washed twice with HBSS, incubated with 45 μM sodium pyrithione and 5 μM $ZnCl_2$, washed again, and imaged. Epifluorescence (A and B) and phase contrast (C and D) images are shown. Scale bar, 20 μm.

among the carboxyl-substituted sensors reported here, but is significantly lower than that of the parent Zinpyr-1 molecule (pK_a = 8.4). The decrease in protonation of the benzylic amine at physiological pH has been suggested to result in a lower quantum yield of the free dye and thereby greatly decreased background fluorescence, offering a plausible explanation for the enhanced fluorescence response discussed above [31]. A ZP1 amide [28], however, displays a similarly enhanced fluorescence response despite having a benzylic amine pK_a nearly identical to that of ZP1. This result suggests that the diminution in fluorescence following substitution of the bottom ring stems from another source. The energy of the benzoic acid moiety of fluorescein and its derivatives plays an important role in determining the fluorescence quantum yield [32], and it is plausible that substitution with a carboxylate modulates the electron transfer driving force so as to give rise to the differences observed here. The pK_a value at 1.5–2.1 probably represents protonation of the xanthene system, which quenches fluorescence. In this protonation state, the positive charge is delocalized over the xanthene ring, but a significant portion resides on the carbon at the 1 position. Thus, an electron-withdrawing substituent para to this carbon (at the 5 position) destabilizes the cation, as reflected in the significantly lowered pK_a value of ZP1(5-CO_2R). Figure 3C displays pH profiles for **4a** and **4b**.

The selectivity of metal response mirrors that of Zinpyr-3, a similar sensor containing fluorine atoms in place of the 2′,7′-chlorine substituents; biologically relevant metal ions produced no significant effect on Zn^{2+} response in background levels up to 10 mM [31]. Most first-row transition metal ions quenched fluorescence in a manner that was not reversed upon addition of excess Zn^{2+}, with the exception of Mn^{2+}, which quenched fluorescence reversibly. The Cd^{2+} ion also produced a large fluorescence enhancement, similar to that of the Zn^{2+} response. Representative data for ZP1(6-CO_2H) are provided in Figure 3D.

Incubation of ZP1 with COS-7 cells affords a Golgi-associated punctate pattern with minimal staining of the remaining cell soma [23]. Treatment of HeLa cells with 5 μM dye for 30 min and subsequent fluorescence microscopic imaging indicated that the ZP1(5/6-CO_2H) derivatives are not taken up by the cell (not shown). The ZP1(5/6-CO_2Et) esters, however, readily stained cells in a pattern similar to that observed following ZP1 treatment (Figure 4). In this experiment, the cells were treated with Zn^{2+} and pyrithione after incubation with either sensor. The apparent permeation of both sensors into intracellular compartments may reflect incomplete hydrolysis of the esters over the time of incubation. The relative in vivo staining of rat hippocampus with ZP1 or ZP1(6-CO_2Et), imaged 12–24 hr after intracranial dye administration, was investigated (Figure 5). Pilocarpine seizures were induced in some rats, and the mechanically injured area near the injection site was examined in rats with or without prior seizures. ZP1 affords a bright granular staining in the zinc-rich neuropil of the hilus, whereas ZP1(6-CO_2Et) staining of this area is much less intense. Hilar neurons injured by seizure accumulate Zn^{2+} in the cytosol and are stained brightly by both dyes, but the punctate staining of the surrounding neuropil obtained with ZP1 lowers the contrast relative to the somata and dendrites, affording little resolution of the underlying neuronal structure (Figure 5G). In contrast, injured neurons stained by ZP1(6-CO_2Et) are clearly delineated, and individual processes can be visualized (Figure 5C). A similar contrast is observed in the staining patterns of the stratum lucidum (SL) and the stratum pyrimidale (SP). ZP1 affords bright punctate staining of the SL, presumably arising from giant (2–10 μm) zinc-containing synaptic terminals of the mossy fibers (Figures 5F and 5H). Much weaker punctate staining is observed in ZP1(6-CO_2Et)-stained SL (Figures 5B and 5D) in comparison to the injured neurons. Figure 6 shows a detailed image of post-seizure CA3 staining by ZP1(6-CO_2Et) in which some punctate staining of vesicular Zn^{2+} is seen. We interpret these results to signify intracellular cleavage of the ethyl ester to give the membrane-impermeant species ZP1(6-CO_2H), which does not penetrate the vesicular membrane. The presence of some punctate staining probably reflects slow ester hydrolysis relative to passive diffusion of the sensor across vesicle membranes. In addition, axons coursing distal to the damage inflicted by the act of injection were brightly and clearly labeled by ZP1(6-CO_2Et) but much less markedly by ZP1, presumably reflecting injury-induced mobilization of zinc from cytosolic metalloproteins in degenerating axons. Seizure or mechanically injured neurons in the stratum pyrimidale are once again much more clearly delineated by ZP1(6-CO_2Et) than the parent ZP1 sensor.

Significance

A generally applicable synthetic route to Zinpyr-1 molecules containing an ester or acid functionality at

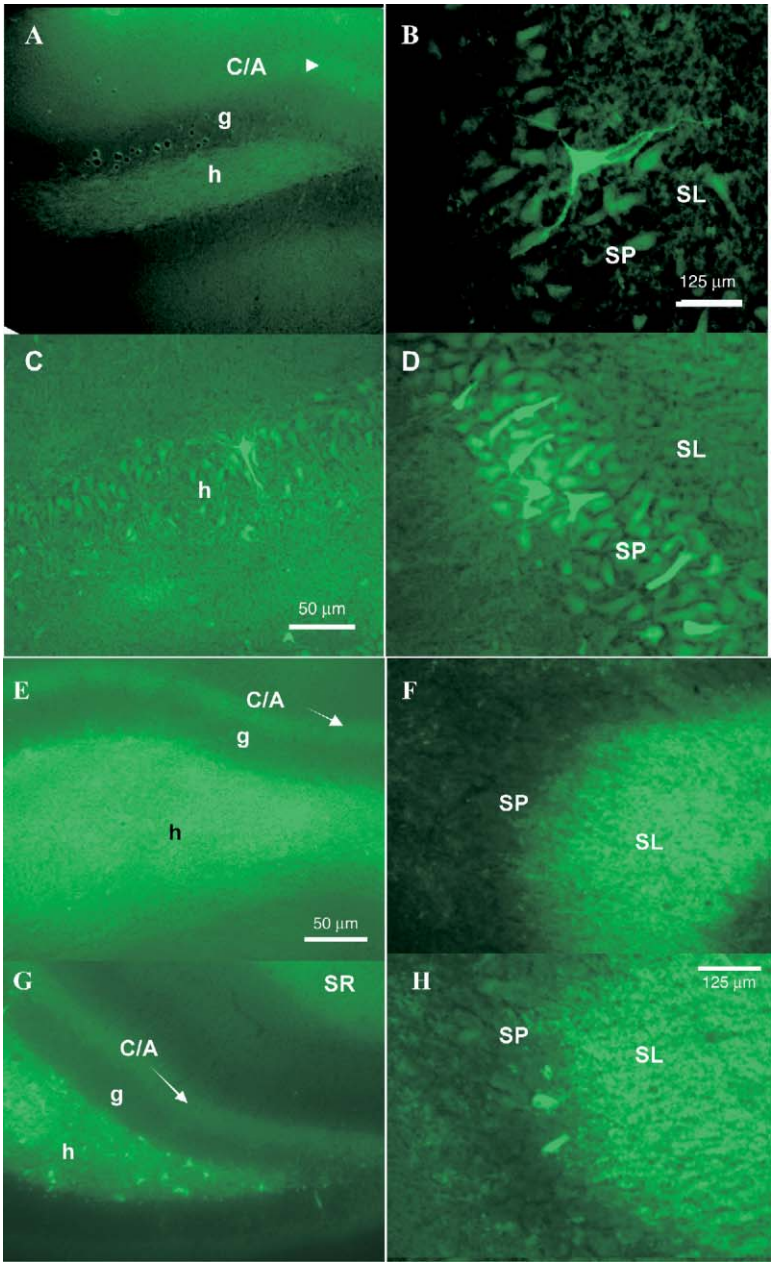

Figure 5. Imaging of ZP1(6-CO_2Et)- and ZP1-Stained Rat Hippocampus

(A), (B), (C), and (D) show ZP1(6-CO_2Et) staining and (E), (F), (G), and (H) show ZP1 staining. Images of normal (A, B, E, and F) and post seizure (C, D, G, and H) brains are shown. Very weak staining of hilar and CA1 neuropil is seen in (A), just able to be discriminated from the granule stratum (g). Neurons injured by the dye injection and sequella stain vividly (B). ZP1 treatment of normal rat (E and F) and post-seizure rat (G and H) affords bright punctate staining of the zinc-rich neuropil in the hilus (H), stratum radiatum (SR), and stratum lucidum (SL) and in the commissural/associational neuropil (C/A), while the granule neuron stratum (g) remains unstained. Scattered stained pyramidal neurons are seen in the hilus of (C) and (G) and stratum pyramidale (SP) of (D) and (H). Scale bars, 125 μm in (A), (C), (E), and (G); 50 μm in (B), (D), (F), and (H).

the 5 or 6 position has been described. Physical characterization of these compounds indicates that the additional group modulates the photophysical properties of these sensors and significantly decreases background fluorescence. Both isomers are suitable for Zn^{2+} sensing. Comparison of sensors containing a free acid or analogous ethyl ester indicates that an additional negative charge renders the sensor membrane impermeable. The presence of a hydrolyzable ester alters subcellular distribution of a sensor in vivo over a 12–24 hr time scale, although no significant differences in subcellular distribution were observed in tissue culture imaging experiments with 30 min incubation periods. This result suggests that the incubation conditions are significant in the subcellular distribution of sensors containing alkyl esters. In summary, we have reported bright fluorescent Zn^{2+} sensors with low-energy visible excitation wavelengths and hybrid subcellular distribution properties. The sensors are mainly trapped in the cytosol, a property not previously available for the Zinpyr family of fluorescein-derivatized zinc ion sensors.

Experimental Procedures

Reagents were purchased from Aldrich and used without further purification. ^1H and ^{13}C NMR spectra were acquired on a Varian 300 or 500 MHz or a Bruker 400 MHz spectrometer. Personnel at the DCIF at MIT acquired HRMS spectra on an FTMS electrospray instrument. Acetonitrile and dichloromethane were obtained from a dry-still solvent dispensation system. Fluorescence spectra were

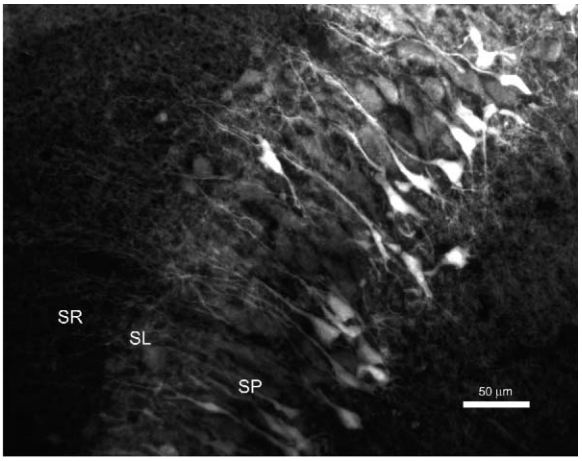

Figure 6. Detail of ZP1(6-CO_2Et) Imaging of the CA3 Region after Pilocarpine-Induced Seizure

The stratum radiatum (SR), stratum lucidum (SL), and stratum pyramidale (SP) are labeled. Scale bar, 50 μm. Note stained pyramidal neurons, unstained stratum lucidum.

measured on a Hitachi F-3010 fluorimeter and UV-visible spectra on a Cary 1E UV-visible spectrophotometer. Both were analyzed by Kaleidagraph 3.0 for Windows.

HeLa cells were grown at 37°C under a 5% CO_2 atmosphere in Dulbecco's modified Eagle's medium (DMEM; Gibco/BRL) supplemented with 10% fetal bovine serum, 1× penicillin/streptomycin and 2 mM L-glutamine. Cells were plated 24 hr before study into 6-well plates containing 2 ml of DMEM per well. Cells were approximately 50% confluent at the time of study. A 10 μl aliquot of dye (1 mM in DMSO) or control (DMSO) was added to each 2 ml well, and the cells were incubated for 30 min at 37°C, at which point the medium was removed and the cells were washed twice with Hanks' buffered salt solution (HBSS) and suspended in 2 ml of DMEM. A 10 μl aliquot of a solution containing 1 mM $ZnCl_2$ and 9 mM sodium-pyrithione in 9:1 DMSO:H_2O was added to selected wells, and the cells were incubated for 10 min at 37°C. The cells were washed again with HBSS, resuspended in HBSS, and imaged by using a Nikon Eclipse TS100 microscope illuminated with a Chiu Mercury 100 W lamp, equipped with an RT Diagnostics camera and operated with Spot Advanced software. Magnification was 20×. Fluorescence images were recorded with a FITC-HYQ filter cube (excitation 460–500, bandpass 510–560 nm).

Male Sprague-Dawley rats weighing 250–500 g were deeply anesthetized with isoflurane, and a small burr hole was opened over the hippocampus (L3.0, P3.0) through which the dura was punctured. Stock solutions of ZP1 or ZP1(6-CO_2Et) (5 or 10 mM in DMSO) were microinfused directly into the brains of the rats with either a Hamilton microliter syringe or a glass pipette (tip ~50–100 μm) connected to a syringe pump. Volumes of 2–4 μl were delivered at 0.5 μl/min by micro syringe (27 gauge needle) or by a Harvard Apparatus syringe pump, using a glass micropipette with the tip broken to 100 μm diameter. All infusions were stereotaxically aimed at the dorsal hippocampus L3, P3, 4.0 sub dura. After infusion, wounds were closed and the rats were allowed to survive for 12–24 hr. Half of the rats were given pilocarpine after dye infusion (300 mg/kg; ip) and monitored for the occurrence of seizures and status epilepticus. In all, tissue from 12 rats was examined in the microscope (3 rats from each of ZP1 control and pilocarpine; ZP1(6-CO_2Et), control and pilocarpine). For brain removal, rats were rendered unconscious by inhalation of carbon dioxide or isoflurane, then decapitated, and the brains were removed quickly and frozen on a liquid CO_2 evaporation freezing stage. After cryotoming at 20 or 30 μm, the sections were allowed to dry briefly on clean glass slides, then viewed and imaged on a Zeiss Universal microscope, either with or without clearing in 100% glycerin and with or without a coverslip. Epi-illumination was provided by a 500 W halogen bulb with band-pass filtering at 480 nm and images were acquired through a 530 nm bandpass and 500 nm dichroic filter using a SPOT II cooled CCD camera. Zeiss 25× (glycerin immersion) and an Olympus 10× planapo objectives were used.

2′,7′-Dichloro-5(6)-Carboxyfluorescein (1a, 1b**)**

4-Chlororesorcinol (28.8 g, 200 mmol) and 1, 2, 4-benzenetricarboxylic acid (21.0 g, 100 mmol) were combined in 100 ml of methanesulfonic acid and stirred in a 90°C oil bath for 18 hr. The reaction mixture was then poured into 1500 ml of stirred ice water, and the resulting suspension was filtered and washed with H_2O. The filtered solid was resuspended in 1 liter of H_2O, filtered again, and dried under vacuum at 90°C overnight to give 40.0 g of an orange solid (90% yield). ^{1}H NMR (methanol-d_4): δ 6.82 (s, 2 H), δ 6.85 (s, 2 H), δ 6.95 (s, 2 H), 6.99 (s, 2 H), δ 7.40 (d, 1 H), δ 7.85 (s, 1 H), δ 8.22 (d, 1 H), δ 8.39 (d, 1 H), δ 8.45 (d, 1 H), δ 8.70 (s, 1 H). The product was carried forward without further purification or characterization.

3′,6′-Diacetyl-2′,7′-Dichloro-6-Carboxyfluorescein Pyridinium Salt (2a**)**

2′,7′-Dichlorofluorescein-5(6)-carboxylic acid (40.0 g, 90 mmol) was stirred in 150 ml of acetic anhydride and 9 ml of pyridine and heated to reflux for 30 min. The reaction was allowed to cool to RT for 4 hr and then filtered. The obtained solid was dried under vacuum to give 16.0 g (30%) of the desired product. ^{1}H NMR ($CDCl_3$): δ 11.13 (br s, 2 H); 8.70 (m, 2 H); 8.42 (d, 1 H); 8.14 (d, 1 H); 7.90 (m, 2 H); 7.46 (m, 2 H); 7.17 (s, 2 H); 6.87 (s, 2 H); 2.36 (s, 6 H). ^{13}C NMR ($CDCl_3$): δ 168.4, 168.3, 152.4, 150.1, 149.0, 147.5, 139.2, 139.1, 132.6, 129.3, 129.1, 126.1, 125.8, 125.2, 123.2, 117.5, 113.3, 21.1. m.p. >300°C (dec).

3′,6′-Diacetyl-2′,7′-Dichloro-5-Carboxyfluorescein (2b**)**

The mother liquor from **2a** was added slowly to 300 ml of stirred H_2O, stirred for an additional 10 min, and extracted with 3× 150 ml of ethyl acetate. The combined organics were washed with 1× 100 ml of 3% HCl and 1× 100 ml brine, dried over $MgSO_4$, and evaporated to give a light brown solid residue, which was recrystallized twice from CH_2Cl_2/EtOAc to give 13.5 g of the desired product (27% yield). ^{1}H NMR ($CDCl_3$): δ 8.84 (s, 1 H); 8.49 (d, 1 H); 7.35 (d, 1 H); 7.19 (s, 2 H); 6.89 (s, 2 H); 2.38 (s, 6 H). ^{13}C NMR ($CDCl_3$): δ 169.7, 169.0, 167.4, 156.3, 149.6, 148.7, 137.3, 132.3, 128.9, 128.1, 126.3, 124.6, 123.0, 116.8, 113.0, 80.8, 66.3, 20.9. m.p. 178°C–180°C.

3′,6′-Diacetyl-2′,7′-Dichlorofluorescein-6-Carboxylate Ethyl Ester (3a**)**

3′,6′-Diacetyl-2′,7′-dichloro-6-carboxyfluorescein pyridinium salt (**2a**, 1.05 g, 1.7 mmol) was dissolved in 30 ml of dichloromethane and the solution was stirred at 0°C. Dimethylformamide (400 μl) and oxalyl chloride (1.7 ml of a 2 M solution in dichloromethane) were added and the reaction was stirred overnight at RT. Sodium carbonate (180 mg, 1 mmol) and ethanol (10 ml) were added, and stirring was continued for 4 hr. The solvents were removed by rotary evaporation and the resulting residue was taken up in CH_2Cl_2, filtered through a short plug (2 cm) of silica gel, and crystallized from dichloromethane/ethyl acetate to give 631 mg (67%) of off-white crystals. ^{1}H NMR ($CDCl_3$): δ 8.38 (d, 1 H); 8.13 (d, 1 H); 7.82 (s, 1 H); 7.17 (s, 2 H); 6.83 (s, 2 H); 4.40 (q, 2 H); 2.38 (s, 6 H); 1.41 (t, 3 H). ^{13}C NMR ($CDCl_3$): δ 167.92; 167.55; 164.61; 151.91; 149.69; 148.68; 137.55; 132.03; 129.00; 125.83; 125.21; 122.91; 117.00; 113.00; 80.87; 62.41; 20.94; 14.56. m.p. 212°C –214°C. HRMS(M+H): Calcd for $C_{27}H_{19}Cl_2O_9$ 557.0406; found 557.0393.

3′,6′-Diacetyl-2′,7′-Dichlorofluorescein-5-Carboxylate Ethyl Ester (3b**)**

3′,6′-Diacetyl-2′,7′-dichloro-5-carboxyfluorescein (**2b**, 527 mg, 1 mmol) was dissolved in CH_2Cl_2 and stirred under nitrogen in a dry ice-acetone bath. DMF (200 μl) was added, followed by oxalyl chloride (1 ml of a 2 M solution in CH_2Cl_2) slowly over a period of 20 min. The solution was stirred for 12 hr, at which time ethanol (10 ml) and $NaHCO_3$ (84 mg, 1 mmol) were added. The reaction was stirred for an additional 4 hr, then evaporated under reduced pres-

sure, taken up in CH_2Cl_2, and filtered through a 2 cm plug of silica gel. Evaporation gave 390 mg of white crystalline residue (70% yield). ^{1}H NMR ($CDCl_3$): δ 8.75 (s, 1 H); 8.43 (d, 1 H); 7.32 (d, 1 H); 7.19 (s, 2 H); 6.85 (s, 2 H); 4.44 (q, 2 H); 2.33 (s, 6 H); 1.44 (t, 3 H). ^{13}C NMR ($CDCl_3$): δ 168.01, 167.82, 164.73, 155.40, 149.75, 148.80, 136.96, 133.68, 129.00, 127.38, 126.31, 124.45, 123.08, 117.08, 113.12, 80.84, 62.32, 21.05, 14.74. HRMS (M+H): Calcd for $C_{27}H_{19}Cl_2O_9$ 557.0406, found 557.0401.

ZP1(6-CO_2H) (4a)
Dipicolylamine (640 mg, 3.2 mmol) was combined with paraformaldehyde (192 mg, 6.4 mmol) in 20 ml of acetonitrile and heated to reflux for 45 min. 3′,6′-Diacetyl-2′,7′-dichloro-6-carboxyfluorescein pyridinium salt (**2a**, 304 mg, 0.5 mmol) was dissolved in 10 ml of MeCN and added, followed by 10 ml of H_2O, and reflux was continued for 24 hr. The resulting suspension was cooled and filtered to yield 360 mg of a light pink powder, which was recrystallized from ethanol to give 282 mg (64% overall) after drying overnight at 60°C under vacuum. The filtrate was acidified with several drops of glacial acetic acid, allowed to stand overnight, and filtered to yield an additional 65 mg (98% crude yield). ^{1}H NMR (DMSO-d_6): δ 8.55 (d, 4 H); 8.22 (d, 1 H); 8.10 (d, 1 H); 7.77 (m, 5 H); 7.39 (d, 4 H); 7.28 (m, 4 H); 6.63 (s, 2 H); 4.16 (s, 4 H); 4.01 (s, 8 H).; ^{13}C NMR (DMSO-d_6): 167.60, 166.11, 157.41, 155.49, 151.7, 148.69, 148.16, 137.45, 131.27, 129.52, 126.78, 125.65, 124.85, 123.23, 122.64, 116.25, 111.97, 109.36, 82.82, 58.65, 48.86. m.p. 215°C–218°C. HRMS (M+H): Calcd for $C_{47}H_{37}Cl_2N_6O_7$ 867.2101; found 867.2080. Anal: Calcd for $C_{47}H_{36}Cl_2N_6O_7$: C, 65.06; H, 4.18; N, 9.69; Cl, 8.17. Found: C, 64.74; H, 3.96; N, 9.61; Cl, 8.29.

ZP1(5-CO_2H) (4b)
3′,6′-Diacetyl-2′,7′-dichloro-6-carboxyfluorescein (264 mg, 0.5 mmol) was subjected to the reaction conditions described for **4a**. The resulting red solution was acidified with several drops of glacial acetic acid, allowed to stand overnight at 4°C, and filtered to yield 361 mg (83% crude yield) of a dark pink crystalline solid, which gave 318 mg on recrystallization from ethanol (73% overall yield). ^{1}H NMR (DMSO-d_6): δ 8.53 (d, 4 H); 8.37 (s, 1 H); 8.30 (d, 1 H); 7.77 (td, 4 H); 7.45 (d, 1 H); 7.37 (d, 4 H); 7.28 (m, 4 H); 6.67 (s, 2 H); 4.16 (s, 4 H); 4.00 (s, 8 H); ^{13}C NMR (DMSO-d_6): 167.58, 166.16, 158.37, 155.77, 154.97, 149.17, 148.69, 137.20, 136.49, 133.25, 126.94, 126.15, 124.73, 123.23, 122.68, 116.47, 112.00, 109.25, 82.65, 58.49, 48.81. m.p. 195°C–195°C. HRMS (M+H): Calcd for $C_{47}H_{37}Cl_2N_6O_7$: 867.2101; found 867.2108. Anal: Calcd for $C_{47}H_{36}Cl_2N_6O_7$: C, 65.06; H, 4.18; N, 9.69; Cl, 8.17. Found: C, 64.83; H, 4.02; N, 9.85; Cl, 8.33.

ZP1(6-CO_2Et) (5a)
3′,6′-Diacetyl-2′,7′-dichlorofluorescein-6-carboxylate ethyl ester (264 mg, 0.47 mmol) was subjected to the same reaction conditions as described for **4a**. The reaction solution was acidified with 5 drops of glacial acetic acid and cooled to –10°C for 30 hr. The resulting salmon-pink precipitate was filtered to give 233 mg (55%) after washing with water and acetonitrile. Recrystallization from ethanol gave 44% yield (185 mg). ^{1}H NMR (DMSO-d_6): δ 8.63 (d, 4 H); 8.35 (d, 1 H); 8.21 (d, 1 H); 7.90 (s, 1 H); 7.86 (t, 4 H); 7.47 (d, 4 H); 7.37 (m, 4 H); 6.71 (s, 2 H); 4.35 (q, 2 H); 4.25 (s, 4 H); 4.09 (s, 8 H); 1.32 (t, 3 H). m.p. 203°C–205°C. HRMS(M+H): Calcd for $C_{49}H_{41}Cl_2N_6O_7$: 895.2414; found 895.2391. Anal: Calcd for $C_{49}H_{40}Cl_2N_6O_7$: C, 65.70; H, 4.50; N, 9.38; Cl, 7.92. Found: C, 65.63; H, 4.37; N, 9.61; Cl, 8.07.

ZP1(5-CO_2Et) (5b)
3′,6′-Diacetyl-2′,7′-dichlorofluorescein-5-carboxylate ethyl ester (141 mg, 0.25 mmol) was subjected to the same reaction conditions as reported for **4a**. The reaction solution was acidified with 5 drops of glacial acetic acid, concentrated on the rotary evaporator, and the resulting pink residue was taken up in MeCN and filtered to give 113 mg of a pink powder (50%) after washing with water and acetonitrile. Recrystallization of 100 mg from EtOH gave 80 mg of a salmon-pink solid. ^{1}H NMR (DMSO-d_6): δ 8.54 (d, 4 H); 8.41 (s, 1 H); 8.33 (dd, 1 H); 7.77 (td, 4 H); 7.49 (d, 1 H); 7.38 (d, 4 H); 7.29 (m, 4 H); 6.67 (s, 2 H); 4.39 (q, 2 H); 4.16 (s, 4 H); 4.00 (s, 8 H); 1.37 (t, 3 H). ^{13}C NMR (DMSO-d_6): δ 168.53, 165.66, 158.45, 156.84, 156.24, 149.80, 149.23, 138.30, 137.19, 133.24, 128.03, 127.10, 126.05, 124.31, 123.78, 118.16, 117.51, 113.08, 110.20, 83.81, 62.62, 59.57, 49.88, 15.29. m.p. 178°C–180°C. HRMS(M+H): Calcd for $C_{49}H_{41}Cl_2N_6O_7$: 895.2414; found 895.2406.

Spectroscopic Measurements
All glassware was washed sequentially with 20% HNO_3, deionized water, and ethanol before use. Purified water (resistivity 18.2 Ohms) was obtained from a Millipore Milli-Q water purification system. Fluorophore stock solutions in DMSO were made up to concentrations of 1 mM and kept at 4°C in 100–500 μl aliquots. Portions were thawed and diluted to the required concentrations immediately prior to each experiment. Fluorescence and absorption data were measured in HEPES buffer (50 mM, pH 7.5, KCl 100 mM) except for the fluorescein standard in quantum yield measurements. Solutions were transferred to clean, dry propylene containers for storage and were filtered (0.25 μm) before data acquisition. Fluorescence spectra were measured from 475 nm to 650 nm. All measurements were performed in triplicate. Dissociation constants were determined by using a dual-metal buffering system as previously described [29].

Extinction Coefficients
A 2 ml portion of HEPES buffer was titrated with 2 μl aliquots of 1 mM fluorophore stock solution and the absorption measured at each concentration. The absorbance at the maximum was plotted as a function of concentration, and the slope was taken as the extinction coefficient. The procedure was repeated using 1.9 ml portions of HEPES buffer containing 100 μl aliquots of 10 mM $ZnCl_2$ solution.

Quantum Yields
Quantum yields were calculated by recording UV-vis spectra of the fluorophore under study and a 1 μM fluorescein standard in 0.1 N NaOH to determine the wavelength where the sample and fluorescein absorption were equal. The fluorescence spectrum of each was then recorded, exciting at the wavelength determined by UV-vis spectral comparison. The integrated emission of the sample was normalized to the fluorescein standard and multiplied by the standard quantum yield of 0.95 [33].

Fluorescence-Dependent pK_a Determination
pK_a titrations were performed in 100 mM KCl, 1 mM EDTA. A 1 mM stock solution of the fluorophore was diluted with 20 ml of this solution to a final concentration of 1 μM. The pH was brought to 11.0 with 45% w/v KOH, then gradually lowered to pH 2, and the fluorescence spectrum was recorded at each half-unit step in pH. The integrated emission area F was normalized, plotted as a function of pH, and fit to the expression in equation 1. Where necessary, individual portions of the plot were fit as a function of a single pK_a in order to determine suitable initial values.

$$\frac{(F - F_0)}{(F_{max} - F_0)} = \left(\frac{\Delta F_{1max}}{[1 + 10^{(pH - pK_{a1})}]}\right) + \left(\frac{\Delta F_{2max}}{[1 + 10^{(pH - pK_{a2})}]}\right) + \left(\frac{\Delta F_{3max}}{[1 + 10^{(pH - pK_{a3})}]}\right) \quad (1)$$

Dissociation Constant Determination
Solutions containing 1 μM fluorophore, 2 mM $CaCl_2$, 1 mM EDTA, and 0 or 1 mM $ZnCl_2$ were prepared as previously described [29]. These solutions were combined to give 3 ml aliquots containing 0–0.9 mM $ZnCl_2$, and were allowed to equilibrate at RT for 20 min. The fluorescence spectrum of each aliquot was measured and the integrated emission was normalized and plotted as a function of effective free Zn^{2+}. The plots were then fit to equation 2.

$$\frac{(F - F_0)}{(F_{max} - F_0)} = k\frac{[Zn^{2+}]_{eff}}{K_d + [Zn^{2+}]_{eff}} \quad (2)$$

Metal Ion Selectivity
The fluorescence spectrum of a 2 ml aliquot of 1 μM fluorophore excited at 512 nm was acquired by itself, after addition of a 4 μl ($CaCl_2$, $MgCl_2$, 1.00 M) or 10 μl (NaCl 2.00 M, $MnSO_4$, $CoCl_2$, $NiCl_2$, $CuCl_2$, $CdCl_2$ 10 mM) aliquot of metal stock solution, and after addi-

tion of a 10 μl aliquot of $ZnCl_2$ (10 mM). The integrated emission of each spectrum was normalized to that of the metal-free control spectrum.

Acknowledgments

This work was supported by the NIGMS (GM65519 to S.J.L.) and by NINDS (NS38585, NS41682, and NS42882 to C.J.F.). Instrumentation in the Department of Chemistry Instrumentation Facility (DCIF) at MIT was funded in part through grants from the NSF (CHE-9808061, CHE9808063, and DBI-9729592).

Received: July 2, 2004
Revised: September 26, 2004
Accepted: September 29, 2004
Published: December 17, 2004

References

1. Kimura, E., and Aoki, S. (2001). Chemistry of zinc(II) fluorophore sensors. Biometals *14*, 191–204.
2. Jiang, P., and Guo, Z. (2004). Fluorescent detection of zinc in biological systems: recent development on the design of chemosensors and biosensors. Coord. Chem. Rev. *248*, 205–229.
3. Kikuchi, K., Komatsu, K., and Nagano, T. (2004). Zinc sensing for cellular application. Curr. Opin. Chem. Biol. *8*, 182–191.
4. Frederickson, C.J. (1989). Neurobiology of zinc and zinc-containing neurons. Int. Rev. Neurobiol. *31*, 145–238.
5. Palmiter, R.D., and Huang, L. (2004). Efflux and compartmentalization of zinc by members of the SLC30 family of solute carriers. Pflugers Arch. *447*, 744–751.
6. Kambe, T., Yamaguchi-Iwai, Y., Sasaki, R., and Nagao, M. (2004). Overview of mammalian zinc transporters. Cell. Mol. Life Sci. *61*, 49–68.
7. Finney, L.A., and O'Halloran, T.V. (2003). Transition metal speciation in the cell: insights from the chemistry of metal ion receptors. Science *300*, 931–936.
8. Frederickson, C.J., Suh, S.W., Silva, D., Frederickson, C.J., and Thompson, R.B. (2000). Importance of zinc in the central nervous system: the zinc-containing neuron. J. Nutr. *130*, 1471S–1483S.
9. Lopantsev, V., Wenzel, H.J., Cole, T.B., Palmiter, R.D., and Schwartzkroin, P.A. (2003). Lack of vesicular zinc in mossy fibers does not affect synaptic excitability of CA3 pyramidal cells in zinc transporter 3 knockout mice. Neuroscience *116*, 237–248.
10. Palmiter, R.D. (2004). Protection against zinc toxicity by metallothionein and zinc transporter 1. Proc. Natl. Acad. Sci. USA *101*, 4918–4923.
11. Cole, T.B., Robbins, C.A., Wenzel, H.J., Schwartzkroin, P.A., and Palmiter, R.D. (2000). Seizures and neuronal damage in mice lacking vesicular zinc. Epilepsy Res. *39*, 153–169.
12. Suh, S.W., Chen, J.W., Motamedi, M., Bell, B., Listiak, K., Pons, N.F., Danscher, G., and Frederickson, C.J. (2000). Evidence that synaptically-released zinc contributes to neuronal injury after traumatic brain injury. Brain Res. *852*, 268–273.
13. Koh, J.-Y., Suh, S.W., Gwag, B.J., He, Y.Y., Hsu, C.Y., and Choi, D.W. (1996). The role of zinc in selective neuronal death after transient global cerebral ischemia. Science *272*, 1013–1016.
14. Thompson, R.B., Whetsell, W.O., Jr., Maliwal, B.P., Fierke, C.A., and Frederickson, C.J. (2000). Fluorescence microscopy of stimulated Zn(II) release from organotypic cultures of mammalian hippocampus using a carbonic anhydrase-based biosensor system. J. Neurosci. Methods *96*, 35–45.
15. Kimura, E., and Koike, T. (1998). Recent development of zinc-fluorophores. Chem. Soc. Rev. *27*, 179–184.
16. Tsien, R.Y. (1981). A non-disruptive technique for loading calcium buffers and indicators into cells. Nature *290*, 527–528.
17. Tsien, R.Y., Pozzan, T., and Rink, T.J. (1982). Calcium homeostasis in intact lymphocytes: cytoplasmic free calcium monitored with a new, intracellularly trapped fluorescent indicator. J. Cell Biol. *94*, 325–334.
18. Varea, E., Ponsoda, X., Molowny, A., Danscher, G., and Lopez-Garcia, C. (2001). Imaging synaptic zinc release in living nervous tissue. J. Neurosci. Methods *110*, 57–63.
19. Frederickson, C.J., Kasarskis, E.J., Ringo, D., and Frederickson, R.E. (1987). A quinoline fluorescence method for visualizing and assaying the histochemically reactive zinc (bouton zinc) in the brain. J. Neurosci. Methods *20*, 91–103.
20. Zalewski, P.D., Millard, S.H., Forbes, I.J., Kapaniris, O., Slavotinek, A., Betts, W.H., Ward, A.D., Lincoln, S.F., and Mahadevan, I. (1994). Video image analysis of labile zinc in viable pancreatic islet cells using a specific fluorescent probe for zinc. J. Histochem. Cytochem. *42*, 877–884.
21. Snitsarev, V., Budde, T., Stricker, T.P., Cox, J.M., Krupa, D.J., Geng, L., and Kay, A.R. (2001). Fluorescent detection of Zn^{2+}-rich vesicles with zinquin: mechanism of action in lipid environments. Biophys. J. *80*, 1538–1546.
22. Nasir, M.S., Fahrni, C.J., Suhy, D.A., Kolodsick, K.J., Singer, C.P., and O'Halloran, T.V. (1999). The chemical cell biology of zinc: structure and intracellular fluorescence of a zinc-quinolinesulfonamide complex. J. Biol. Inorg. Chem. *4*, 775–783.
23. Burdette, S.C., Walkup, G.K., Spingler, B., Tsien, R.Y., and Lippard, S.J. (2001). Fluorescent sensors for Zn^{2+} based on a fluorescein platform: synthesis, properties and intracellular distribution. J. Am. Chem. Soc. *123*, 7831–7841.
24. Burdette, S.C., Frederickson, C.J., Bu, W., and Lippard, S.J. (2003). ZP4, an improved neuronal Zn^{2+} sensor of the Zinpyr family. J. Am. Chem. Soc. *125*, 1778–1787.
25. Frederickson, C.J., Burdette, S.C., Frederickson, C.J., Sensi, S.L., Weiss, J.H., Yin, H.Z., Balaji, R.V., Truong-Tran, A.Q., Bedell, E., Prough, D.S., et al. (2004). Method for identifying neuronal cells suffering zinc toxicity by use of a novel fluorescent sensor. J. Neurosci. Methods *139*, 79–89.
26. Nolan, E.M., Burdette, S.C., Harvey, J.H., Hilderbrand, S.A., and Lippard, S.J. (2004). Synthesis and characterization of zinc sensors based on a monosubstituted fluorescein platform. Inorg. Chem. *43*, 2624–2635.
27. Sun, W.C., Gee, K.R., Klaubert, D.H., and Haugland, R.P. (1997). Synthesis of fluorinated fluoresceins. J. Org. Chem. *62*, 6469–6475.
28. Woodroofe, C.C., and Lippard, S.J. (2003). A novel two-fluorophore approach to ratiometric sensing of Zn^{2+}. J. Am. Chem. Soc. *125*, 11458–11459.
29. Walkup, G.K., Burdette, S.C., Lippard, S.J., and Tsien, R.Y. (2000). A new cell-permeable fluorescent probe for Zn^{2+}. J. Am. Chem. Soc. *122*, 5644–5645.
30. Selwyn, J.E., and Steinfeld, J.I. (1972). Aggregation equilibria of xanthene dyes. J. Phys. Chem. *76*, 762–774.
31. Chang, C.J., Nolan, E.M., Jaworski, J., Burdette, S.C., Sheng, M., and Lippard, S.J. (2004). Bright fluorescent chemosensor platforms for imaging endogenous pools of neuronal zinc. Chem. Biol. *11*, 203–210.
32. Miura, T., Urano, Y., Tanaka, K., Nagano, T., Ohkubo, K., and Fukuzumi, S. (2003). Rational design principle for modulating fluorescence properties of fluorescein-based probes by photoinduced electron transfer. J. Am. Chem. Soc. *125*, 8666–8671.
33. Brannon, J.H., and Magde, D. (1978). Absolute quantum yield determination by thermal blooming. Fluorescein. J. Phys. Chem. *82*, 705–709.